

PCCP

Accepted Manuscript



This is an *Accepted Manuscript*, which has been through the Royal Society of Chemistry peer review process and has been accepted for publication.

Accepted Manuscripts are published online shortly after acceptance, before technical editing, formatting and proof reading. Using this free service, authors can make their results available to the community, in citable form, before we publish the edited article. We will replace this *Accepted Manuscript* with the edited and formatted *Advance Article* as soon as it is available.

You can find more information about *Accepted Manuscripts* in the [Information for Authors](#).

Please note that technical editing may introduce minor changes to the text and/or graphics, which may alter content. The journal's standard [Terms & Conditions](#) and the [Ethical guidelines](#) still apply. In no event shall the Royal Society of Chemistry be held responsible for any errors or omissions in this *Accepted Manuscript* or any consequences arising from the use of any information it contains.

Cite this: DOI: 10.1039/c0xx00000x

www.rsc.org/xxxxxx

ARTICLE TYPE

Dual use of tantalum disulfides as hole and electron extraction layers in organic photovoltaic cells

Quyết Van Le^a, Thang Phan Nguyen^a, Kyoung Soon Choi^a,
Yoon-Ho Cho^b, Young Joon Hong^c, and Soo Young Kim^{a,*}

Received (in XXX, XXX) Xth XXXXXXXXXX 20XX, Accepted Xth XXXXXXXXXX 20XX

DOI: 10.1039/b000000x

UV/ozone treated (UVO-treated) TaS₂ and non-treated TaS₂ nanosheets are introduced to organic photovoltaic cells (OPVs) as hole extraction layer (HEL) and electron extraction layers (EEL). TaS₂ nanosheets are obtained via ultrasonic vibration and size-controlled by centrifugation. Atomic force microscopy (AFM) images reveal that the thickness and lateral size of TaS₂ nanosheets are approximately 1 and 70 nm, indicating that uniform and ultrathin TaS₂ nanosheets are obtained. The work function of TaS₂ increases from 4.4 eV to 4.9–5.1 eV after applying UVO treatment by forming Ta₂O₅. In addition, the power conversion efficiencies of normal OPV with UVO-treated TaS₂ and inverted OPV with TaS₂ are 3.06 and 2.73 %, which are higher than those of OPV without TaS₂ (1.56 % for normal OPV and 0.22 % for inverted OPV). These results indicate that TaS₂ is a promising material for HEL and EEL layer in OPVs.

1 Introduction

Organic photovoltaic cells (OPVs) have emerged as competitive devices for harvesting clean and sustainable energy in the near future. To date, a power conversion efficiency (PCE) of over 8 % has been obtained,¹⁻³ bringing the actual manufacture of OPVs one step closer to being realized. The performance of OPVs can be improved by sandwiching a buffer layer between the cathode (or anode) and the active layer in order to facilitate electron (or hole) transfer. In normal OPV (N-OPV), poly(3,4-ethylenedioxythiophene):poly(styrene sulfonate) (PEDOT:PSS) is widely used as the hole extraction layer (HEL) owing to its suitable work function (~ 5.0 eV) and ease with which it can be deposited on indium tin oxide (ITO)/glass substrate via solution processing. PEDOT:PSS is, however, highly acidic and hygroscopic and results in damage of the ITO surface. This damage, in turn, leads to rapid degradation of the device.⁴⁻⁶ Various materials such as MoO₃,^{7, 8} NiO,⁹ MoS₂,¹⁰⁻¹² WO₃,¹³ WS₂,¹⁴ and V₂O₅,¹⁵ have, therefore, been investigated in order to overcome these drawbacks of PEDOT:PSS. In the case of inverted OPV (I-OPV), low work function metal oxides such as TiO₂,¹⁶ TiO_x,^{17, 18} ZnO,¹⁷ Cs₂O₃,¹⁹ and Al,²⁰ are used on ITO/glass substrate as an electron extraction layer (EEL) to improve stability of OPVs. Recently, single- and multiple-layered, two-dimensional transition metal dichalcogenides (2-D TMDs) have attracted much attention owing to their superior properties. These properties enable their use in a wide range of applications including photo transistors, field effect transistors, sensor, batteries, hydrogen reactions, water splitting, and solar cells.^{10-12, 14, 21-27} Single layer 2-D TMDs can be obtained through chemical

cleavage, liquid exfoliation, and chemical vapor deposition.²²

Exfoliation by ultrasonic vibration is the simplest method from which 2-D nanosheets can be obtained at room temperature for large scale production. In addition, applications, such as MoS₂ and WS₂ as HEL in OPV, which include 2-D TMDs are both more stable and efficient than PEDOT:PSS.^{10-12, 14}

TaS₂ nanosheets are structurally similar to MoS₂ and WS₂. They are layered compounds with three-coordinate sulfide and trigonal prismatic Ta centers. Each layer is 6-7 Å thick, and consists of a hexagonally packed Ta atom layer sandwiched between two layers of S atoms.²⁸ The sandwich layers are bound by a weak van der Waals force.²⁸ This weak binding force facilitates exfoliation to a single layer by means of ultrasonic vibration. Moreover, the electrical resistivity of TaS₂ is approximately 10⁻³ Ωcm, which is much lower than that of MoS₂ and WS₂ (18 and 0.1 Ωcm).²⁹⁻³¹ It is reported that resistivity of buffer layer plays a vital role on performance of OPVs. Specifically, the lower resistivity of buffer layer results in the higher performance of device.³² TaS₂ should therefore, be a promising candidate for use as buffer layers for OPVs. To this end, 2-D TMDs TaS₂ nanosheets were fabricated in this study by means of ultrasonic vibration and applied to OPVs as HEL and EEL in order to improve the performance of OPVs. The UVO-treatment method was used to modulate the function of TaS₂ from EEL to HEL. The properties of the material and the performance of N-OPV and I-OPV based TaS₂ were investigated and discussed.

2 Experimental section

The synthesis of TaS₂

TaS₂ and *N*-methyl vinylpyrrolidone (NVP) were purchased from Sigma-Aldrich. An ultrasonicator (SONICS VCX-750, Sonicor Microtip Probes) was used to exfoliate the TaS₂. This was done by first dispersing 30 mg of TaS₂ in 10 mL of NVP and then ultrasonically vibrating the resulting solution for 4 hours at 400 W. Afterwards, the samples were centrifuged (DAIHAN WiseSpin[®] CF-10) for 10 min at 5000, 6000, 8000, and 10000 rpm in order to remove the TaS₂ which have large sizes. The floating solution containing the ultra-thin, exfoliated TaS₂ nanosheets was pipetted out and the solvent was removed by repeated washing of the sheets with isopropanol. The final product was dried at 30 °C in a vacuum oven and the resulting powder of TaS₂ nanosheets was dispersed in *N,N*-dimethyl formamide (DMF) for further measurement and thin film coating.

15 The fabrication of N-OPVs

N-OPVs were fabricated using patterned ITO coated glass substrate. The ITO/glass was cleaned with acetone, iso-propyl alcohol, and deionized water for 10 min in an ultrasonic bath and then dried and exposed to UV/ozone (UVO) for 15 min. TaS₂ nanosheets in DMF (1mg/mL) were spin-coated at 3000 rpm for 90 s and dried at 150 °C in air. The UVO treatments were subsequently performed for various periods of time in order to determine the optimum condition. For the sake of comparison, PEDOT:PSS was spin-coated at 4000 rpm for 30 s and annealed for 10 min at 150 °C in air. The thickness of PEDOT:PSS was measured as 40 nm using a Dektack profiler. HEL-coated substrates were then transferred to a N₂ filled glove box for further processing. Furthermore, poly(3-hexylthiophene) and [6,6]-phenyl-C61-butyric acid methyl ester (P3HT:PCBM, 6:4 wt%) were prepared in 1,2-dichlorobenzene with concentration of 30 mg/mL, followed by heating at 60 °C for 12 h. After spin-coating the P3HT:PCBM at 700 rpm for 30 s, the substrate was kept in a petri dish for 1 h, to allow for slow evaporation, and baked at 110 °C for 10 min. Finally, the cathode with LiF (1-nm thickness) and Al (100-nm thickness) were thermally deposited at a base pressure of 2 × 10⁻⁶ Torr. The active area of the resulting device was approximately 4 mm². The schematic structure of N-OPVs based on UVO-treated TaS₂ is shown in Fig. 1(a).

Fabrication of I-OPVs

The I-OPVs were fabricated into an ITO/glass/TaS₂ (TiO_x)/P3HT:PCBM/MoO₃/Al structure (Fig. 1(b)). The substrate and active layer were prepared following the same procedure that was used to produce the N-OPVs. In this case, however, the TaS₂ layer was annealed in a glove box in order to avoid oxidation. For the sake of comparison with TaS₂, sol-gel TiO_x solution was spin-coated at 3000 rpm and then dried at 150 °C in air. The process was completed by thermally depositing 1 nm thick MoO₃ and 100 nm thick Al on top of P3HT:PCBM at a base pressure of 2 × 10⁻⁶ Torr.

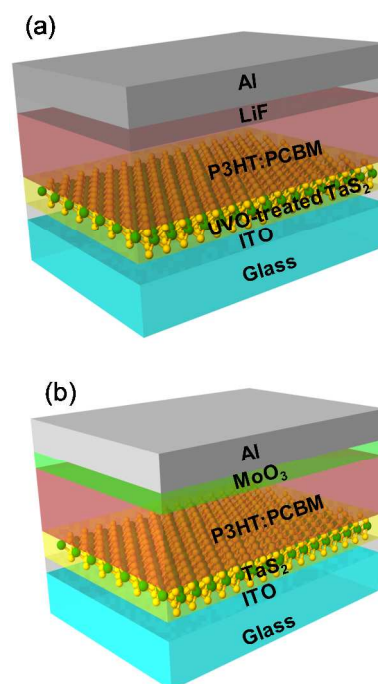
50 Characterization

Ultraviolet (UV)-vis absorption spectra (V-670 UV-vis spectrophotometer) were collected in order to confirm the change in size of TaS₂. Similarly, contact mode atomic force microscopy (AFM, XE-100/PSIA) was used to determine the thickness of the

exfoliated TaS₂. Synchrotron radiation photoemission spectroscopy (SRPES) experiments were also performed. These were conducted in an ultra-high-vacuum chamber (base pressure of ≈10⁻¹⁰ Torr) at a 4D beam line in the Pohang Acceleration Laboratory. The onset of photoemission, corresponding to the vacuum level at the surface of TaS₂, was measured using an incident photon energy of 250 eV with a negative bias on the sample. The results were corrected for charging effects by using Au 4f as an internal reference. The current density–voltage (*J*–*V*) curve was measured with a Keithley 2612 source meter under 65 AM 1.5 G illumination (100 mW/cm²). The corresponding maximum power conversion efficiency (PCE) for the conversion of solar radiation to electrical power was then calculated using the equation

$$\frac{V_{oc} \times J_{sc} \times FF}{P_{in} (= 100 \text{ mW/cm}^2)} \times 100,$$

where *V*_{oc} is the open-circuit voltage, *J*_{sc} is the short-circuit current density, *FF* is the fill factor, and *P*_{in} is the illumination power.



75 Fig.1 Schematic structures of (a) N-OPV and (b) I-OPV based on TaS₂.

3 Results and discussion

Figure 2(a) shows the change of peak positions in the UV-vis spectra for different centrifugation speeds. The peak that appears at 641 nm in the bulk material corresponds to a band gap of 1.9 eV. According to previous reports, absorption peaks originate from the excitation state of the metal in MoS₂ and WS₂ materials.^{33, 34} Since TaS₂ has a similar structure to that of MoS₂ and WS₂, the peak at 641 nm is assumed to come from the bonding between 4f and 3p orbitals of the sulfur atom. The peak position decreases from 593 nm (2.09 eV) to 472 nm (2.63 eV) with increasing speeds in the range of 5000 to 10000 rpm (Figure 2(a)). This decrease is indicative of a reduction in particle size.

There was, however, no significant decrease of wavelength for speeds higher than 10000 rpm. This suggests a saturation of the effect of centrifugation speed in obtaining uniform and ultra-thin TaS₂ nanosheets. A speed of 10000 rpm was, therefore, used for further characterization and device fabrication. The TaS₂ on the SiO₂/Si substrate was also imaged by AFM (Figure 2(b)). Figure 2(b) reveals that centrifuging resulted in uniform and fully covered ultrathin TaS₂ nanosheets. The height difference of the TaS₂ nanosheets was measured along the red line in the AFM image and the thickness and lateral size were measured as approximately 1 and 70 nm, respectively. This lateral size (70 nm) is much smaller than that obtained from the lithium intercalation exfoliation method.³⁵ These results, therefore, indicate that bulk TaS₂ was exfoliated into uniform TaS₂ nanosheets by means of ultrasonic vibration.

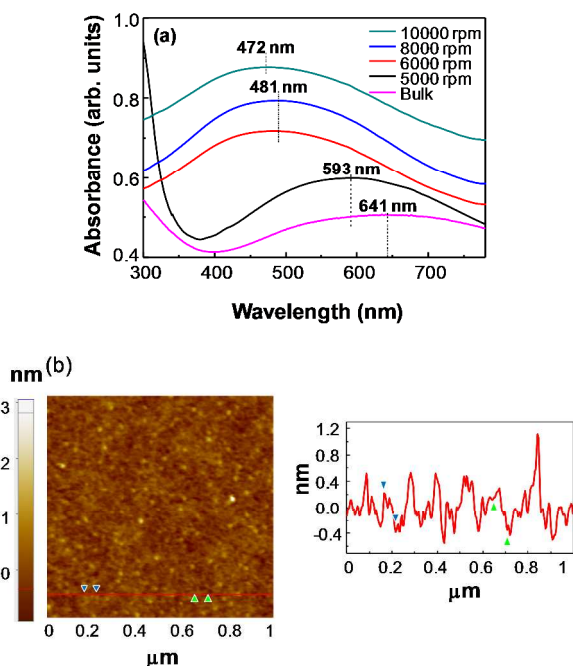


Fig. 2 (a) UV-vis absorption spectra of TaS₂ bulk and TaS₂ nanosheets for various centrifugation speeds. (b) AFM image of TaS₂ nanosheets spin-coated on the SiO₂/Si substrate. The height difference is shown along the red line in the AFM image

The composition of the UVO-treated TaS₂ film was determined by SRPES in order to understand the effect of the treatment on these films (Fig. 3). The Ta 4f peak of the spin-coated nanosheets is composed of two doublets. One of the doublets has binding energies of 24.7 and 26.6 eV which correspond to the Ta⁴⁺ 4f_{7/2} and Ta⁴⁺ 4f_{5/2} of TaS₂, respectively. The two smaller peaks located at 26.9 and 28.8 eV indicate the presence of Ta⁵⁺ 4f_{7/2} and Ta⁵⁺ 4f_{5/2} of Ta₂O₅, which is formed during the fabrication process.^{35, 36} The relative intensity of Ta⁵⁺ 4f increases with UVO treatment time, suggesting the formation of Ta₂O₅. The SRPES spectra of O 1s shown in Fig. 3(b) have two separate peaks, which located at 531.6 and 532.9 eV. The peak centered at 531.6 eV corresponds to the oxygen bonded to Ta⁵⁺ and the peak at 532.9 eV identifies the adsorbed oxygen on the surface.³⁶ It is shown that the peak height with UVO treatment time, for the binding energy of 531.6 eV, confirms that the TaS₂ nanosheets

were partially converted to Ta₂O₅. These results indicate that UVO treatments partially convert TaS₂ nanosheets to Ta₂O₅.

Figure 4 (a) plots the changes in the work function of TaS₂ for various UVO treatment times. The onset of the secondary electron was determined by extrapolating two solid lines from the background and straight onset in the spectra.³⁷ The work function of exfoliated TaS₂ is 4.4 eV. UVO treatments of 15, 30 and 45 min increase this value to 4.9, 5.0 and 5.1 eV, respectively. It is assumed that treating with UVO introduces oxygen into the lattice of TaS₂ thereby forming Ta₂O₅, which, in turn, leads to an increase in the work function. Figure 4(b) and (c) show the schematic band diagram of N-OPV and I-OPV, which, as previously stated, are used as HEL and EEL, respectively. The work functions of ITO, PEDOT:PSS, TiO_x, LiF/Al, and MoO₃ were adopted from the literature.^{8, 11, 14, 20, 38} Based on these work functions, it seems that UVO-treated TaS₂ nanosheets are suitable for HEL, while non-treated TaS₂ nanosheets are suited for EEL.

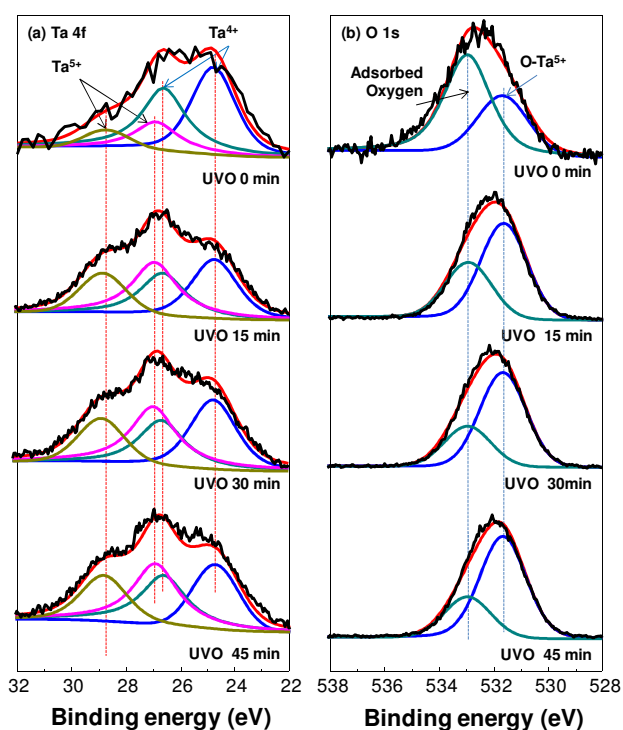


Fig. 3 SRPES spectra of (a) Ta 4f and (b) O 1s peaks for various UVO treatment times.

Table 1 Summary of N-OPV properties as a function of UVO treatment time of TaS₂.

	J _{sc} (mA/cm ²)	V _{oc} (V)	FF (%)	PCE (%)
Bare ITO	7.90	0.40	49	1.56
PEDOT:PSS	8.12	0.62	65	3.28
TaS ₂ UVO 0 min	1.00	0.03	25	0.01
TaS ₂ UVO 15 min	8.09	0.61	61	3.00
TaS ₂ UVO 30 min	7.87	0.61	64	3.06
TaS ₂ UVO 45 min	8.07	0.60	62	3.04

Table 2 Summary of I-OPV properties without EEL and with TiO_x, TaS₂ as EEL.

	J_{sc} (mA/cm ²)	V_{oc} (V)	FF (%)	PCE (%)
Bare ITO	5.75	0.13	28	0.22
TiO _x	8.04	0.55	56	2.50
TaS ₂	8.76	0.60	52	2.73

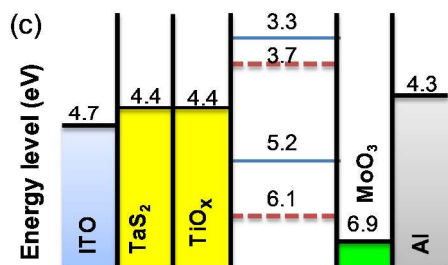
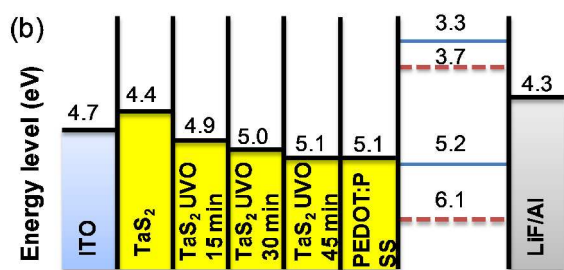
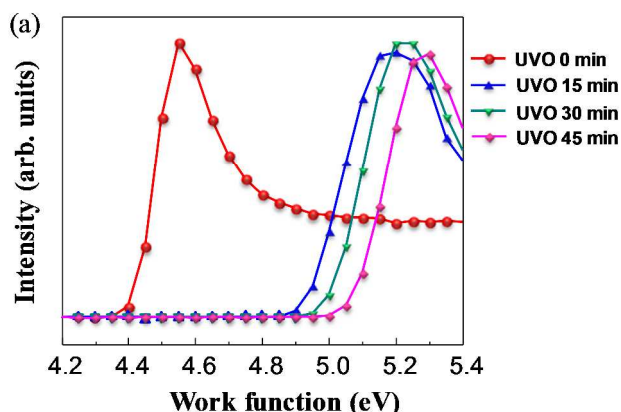
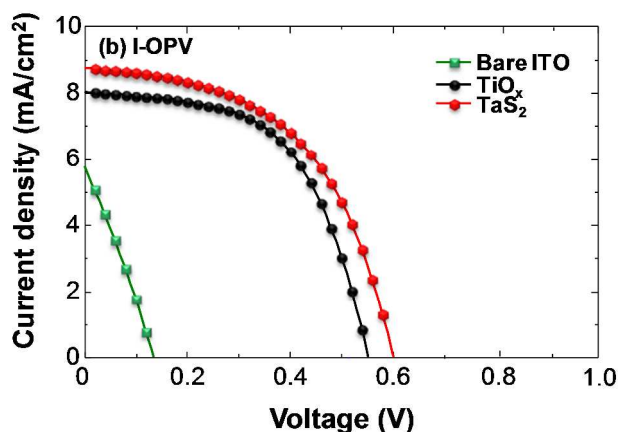
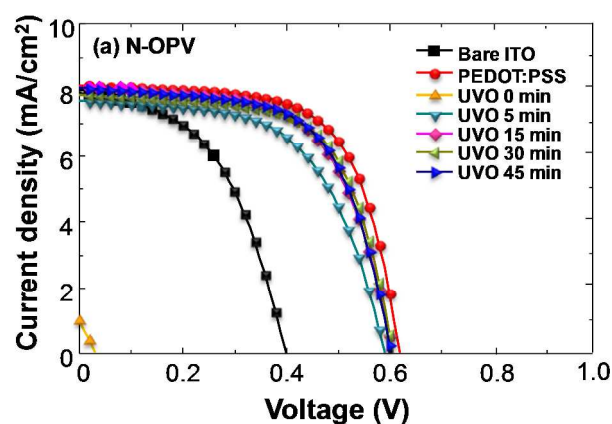
**Fig. 4** Changes of secondary electron spectra of TaS₂ with UVO treatment time. Schematic band diagram of (b) N-OPV and (c) I-OPV.

Figure 5(a) compares the J-V curves of N-OPV based on TaS₂ for various UVO treatment times. N-OPV with bare TaS₂ nanosheets HEL has a PCE value of 0 %. Non-treated TaS₂ nanosheets are, therefore, unsuitable for HEL in OPVs. For reliable values, each experiment was repeated at least 5 times. It is considered that the remnant solvent which was attached on the surface of TaS₂ in the synthesis step deteriorates the performance of OPVs. UVO treatment cleans the surface as well as increases the work function. After performing the UVO treatment for 15 min, the PCE of N-OPV increased to 3 % with $J_{sc} = 8.09$ mA/cm², $V_{oc} = 0.61$ V, and $FF = 61$ %. The PCE then slightly increased to 3.06

20 % ($J_{sc} = 7.87$ mA/cm², $V_{oc} = 0.61$ V, and $FF = 64$ %) after prolonging the UVO treatment time to 30 min. However, no further improvement was observed for UVO treatment times longer than 30 min. This observation suggests that 15 - 30 min is the suitable time for UVO treatment of TaS₂ nanosheets. The TaS₂ nanosheets treated by UVO for 30 min have a work function of 5 eV, which facilitates hole injection from the active layer to the ITO anode. Thus, the PCE of OPVs with UVO-treated TaS₂ is approximately 96 % higher than that of the device based on bare ITO (PCE= 1.56 %, $J_{sc} = 7.9$ mA/cm², $V_{oc} = 0.4$ V, and $FF = 49$ %) and comparable to the value of the PEDOT:PSS-based device (PCE = 3.28 %, $J_{sc} = 8.12$ mA/cm², $V_{oc} = 0.62$ V, and $FF = 65$ %). The device characteristics of N-OPV are summarized in Table I. Fig. 5(b) plots the J-V curve of the I-OPV based on TaS₂. The PCE of OPV without EEL is only 0.22 % owing to the energy difference between the ITO and the active layer. After inserting the TaS₂ nanosheets as EEL, the PCE of I-OPV increased to 2.7 % ($J_{sc} = 8.76$ mA/cm², $V_{oc} = 0.6$ V, and $FF = 52$ %), which is comparable to the device with the well-known TiO_x EEL (PCE=2.5 %, $J_{sc} = 8.04$ mA/cm², $V_{oc} = 0.55$ V, and $FF = 56$ %). The device characteristics of the I-OPV are summarized in Table II. These data suggest that TaS₂ nanosheets can be used as both HEL and EEL in OPVs.

**Fig. 5** (a) J-V characteristics of the N-OPVs for UVO irradiation times on TaS₂ as HEL. (b) J-V characteristics of the I-OPVs using TaS₂ as EEL.

4 Conclusion

Ultrathin TaS₂ nanosheets were produced by means of ultrasonic vibration and applied to OPVs as interfacial layers for both the cathode and anode. The reduction of the UV-vis peak suggested that the layer thickness of TaS₂ decreased upon ultrasonic vibration. Furthermore, AFM imaging revealed that the thickness and lateral size of TaS₂ nanosheets are approximately 1 and 70 nm respectively. UVO treatment of TaS₂ nanosheets resulted in an increase of the work function from 4.4 eV to 4.95 eV. In addition, the PCE of N-OPVs increased from 1.56 to 3.06 % by inserting UVO-treated TaS₂ as HEL. The insertion of non-treated TaS₂ in I-OPV as EEL also improved the PCE from 0.22 to 2.73 %. These results demonstrate that TaS₂ nanosheets are promising candidates for both anode and cathode interfacial layers which can improve the performance of OPV devices through solution processing.

Acknowledgments

This research was supported by the Center for Green Airport Pavement Technology (CGAPT) of Chung-Ang University. This work by Y. J. Hong was supported by the faculty research fund of Sejong University in 2012.

Notes and references

^aSchool of Chemical Engineering and Materials Science, Chung-Ang University 221, Heukseok-dong, Dongjak-gu, Seoul 156-756, Republic of Korea.

^bDepartment of Civil and Environmental Engineering, Chung-Ang University 221, Heukseok-dong, Dongjak-gu, Seoul 156-756, Republic of Korea

^cDepartment of Nanotechnology and Advanced Materials Engineering, Graphene Research Institute, Hybrid Materials Research Center, Sejong University, Gwangjin-gu, Seoul 143-747, Republic of Korea.

*E-mail: sooyoungkim@cau.ac.kr, Tel.: 82-2-820-5875, Fax: 82-2-824-3495.

- Z. He, C. Zhong, X. Huang, W. Y. Wong, H. Wu, L. Chen, S. Su and Y. Cao, *Adv. Mater.*, 2011, **23**, 4636-4643.
- A. K. Kyaw, D. H. Wang, V. Gupta, J. Zhang, S. Chand, G. C. Bazan and A. J. Heeger, *Adv. Mater.*, 2013, **25**, 2397-2402.
- X. Guo, M. Zhang, W. Ma, L. Ye, S. Zhang, S. Liu, H. Ade, F. Huang and J. Hou, *Adv. Mater.*, 2014, **26**, 4043-4049.
- M. P. de Jong, L. J. van IJzendoorn and M. J. A. de Voigt, *Appl. Phys. Lett.*, 2000, **77**, 2255-2257.
- K. Kawano, R. Pacios, D. Poplavskyy, J. Nelson, D. D. C. Bradley and J. R. Durrant, *Sol. Energy Mater. Sol. Cells*, 2006, **90**, 3520-3530.
- M. Jørgensen, K. Norrman and F. C. Krebs, *Sol. Energy Mater. Sol. Cells*, 2008, **92**, 686-714.
- H. Pan, L. Zuo, W. Fu, C. Fan, B. Andreasen, X. Jiang, K. Norrman, F. C. Krebs and H. Chen, *Org. Electron.*, 2013, **14**, 797-803.
- W. J. Dong, G. H. Jung and J.-L. Lee, *Sol. Energy Mater. Sol. Cells*, 2013, **116**, 94-101.
- J. R. Manders, S.-W. Tsang, M. J. Hartel, T.-H. Lai, S. Chen, C. M. Amb, J. R. Reynolds and F. So, *Adv. Funct. Mater.*, 2013, **23**, 2993-3001.
- X. Gu, W. Cui, H. Li, Z. Wu, Z. Zeng, S.-T. Lee, H. Zhang and B. Sun, *Adv. Energy Mater.*, 2013, **3**, 1262-1268.
- Q. V. Le, T. P. Nguyen, H. W. Jang and S. Y. Kim, *Phys. Chem. Chem. Phys.*, 2014, **16**, 13123-13128.
- J.-M. Yun, Y.-J. Noh, J.-S. Yeo, Y.-J. Go, S.-I. Na, H.-G. Jeong, J. Kim, S. Lee, S.-S. Kim, H. Y. Koo, T.-W. Kim and D.-Y. Kim, *J. Mater. Chem. C*, 2013, **1**, 3777.
- S. B. Lee, J. Ho Beak, B. h. Kang, K.-Y. Dong, Y.-Y. Yu, Y. Doo Lee and B.-K. Ju, *Sol. Energy Mater. Sol. Cells*, 2013, **117**, 203-208.
- Q. V. Le, T. P. Nguyen and S. Y. Kim, *Phys. Status Solidi RRL*, 2014, **8**, 390-394.
- V. Shrotriya, G. Li, Y. Yao, C.-W. Chu and Y. Yang, *Appl. Phys. Lett.*, 2006, **88**, 073508.
- Z. Lin, C. Jiang, C. Zhu and J. Zhang, *ACS Appl. Mater. Interfaces*, 2013, **5**, 713-718.
- F. Guillain, D. Tsikritzis, G. Skoulatakis, S. Kennou, G. Wantz and L. Vignau, *Sol. Energy Mater. Sol. Cells*, 2014, **122**, 251-256.
- M. Seßler, A. Saeed, M. Kohlstädt and U. Würfel, *Org. Electron.*, 2014, **15**, 1407-1412.
- G. Li, C. W. Chu, V. Shrotriya, J. Huang and Y. Yang, *Appl. Phys. Lett.*, 2006, **88**, 253503.
- J. Chang, Z. Ming Kam, Z. Lin, C. Zhu, J. Zhang and J. Wu, *Appl. Phys. Lett.*, 2013, **103**, 173303.
- R. Gatensby, N. McEvoy, K. Lee, T. Hallam, N. C. Berner, E. Rezvani, S. Winters, M. O'Brien and G. S. Duesberg, *Appl. Surf. Sci.*, 2014, **297**, 139-146.
- X. Huang, Z. Zeng and H. Zhang, *Chem. Soc. Rev.*, 2013, **42**, 1934-1946.
- T.-Y. Chen, Y.-H. Chang, C.-L. Hsu, K.-H. Wei, C.-Y. Chiang and L.-J. Li, *Int. J. Hydrogen Energy*, 2013, **38**, 12302-12309.
- B. Radisavljevic, A. Radenovic, J. Brivio, V. Giacometti and a. A. Kis, *Nat Nanotech.*, 2011, **6**, 147-150.
- O. Lopez-Sanchez, D. Lembke, M. Kayci, A. Radenovic and A. Kis, *Nat Nanotech.*, 2013, **8**, 497-501.
- S. Li, Z. Chen and W. Zhang, *Mater Lett*, 2012, **72**, 22-24.
- R. Bhandavat, L. David and G. Singh, *J. Phys. Chem. Lett.*, 2012, **3**, 1523-1530.
- M. Chhowalla, H. S. Shin, G. Eda, L.-J. Li, K. P. Loh and H. Zhang, *Nature Chem.*, 2013, **5**, 263-275.
- F. J. Di Salvo and J. E. Graebner, *Solid State Commun.*, 1977, **23**, 825-828.
- A. J. Grant, T. M. Griffiths, G. D. Pitt and A. D. Yoffe, *J. Phys. C: Solid State Phys.*, 1975, **8**, L17.
- T. J. Wieting, *J. Phys. Chem. Solids.*, 1970, **31**, 2148-2151.
- S. H. Oh, S. J. Heo, J. S. Yang and H. J. Kim, *ACS Appl. Mater. Interfaces*, 2013, **5**, 11530-11534.
- B. Visic, R. Dominko, M. Gunde, N. Hauptman, S. Skapin and M. Remskar, *Nanoscale Res. Lett.*, 2011, **6**, 1-6.
- L. Lin, Y. Xu, S. Zhang, I. M. Ross, A. C. M. Ong and D. A. Allwood, *ACS Nano*, 2013, **7**, 8214-8223.
- Z. Zeng, C. Tan, X. Huang, S. Bao and H. Zhang, *Energy Environ. Sci.*, 2014, **7**, 797.
- M. T. Seman, J. J. Robbins, D. Leonhardt, S. Agarwal and C. A. Wolden, *J. Electrochem. Soc.*, 2008, **155**, J168.
- K. S. Choi, Y. Park and S. Y. Kim, *J. Nanosci. Nanotechnol.*, 2013, **13**, 3282-3287.
- J. Meyer, S. Hamwi, M. Kröger, W. Kowalsky, T. Riedl and A. Kahn, *Adv. Mater.*, 2012, **24**, 5408-5427.